Naval Research Laboratory
Washington, DC 20375-5320

NRL/6360/MR—2023/3

Interplay of Strain and Short Range Ordering At Nitride Heterointerfaces

ANDREW C. LANG

Nanoscale Materials Section
Materials Science and Technology Division

May 8, 2023

REPORT DOCUMENTATION PAGE

Form Approved
OMB No. 0704-0188

1. REPORT DATE *(DD-MM-YYYY)*	**2. REPORT TYPE**	**3. DATES COVERED** *(From - To)*
08-05-2023	NRL Memorandum Report	27-09-2021 – 26-09-2022

4. TITLE AND SUBTITLE

Interplay of Strain and Short Range Ordering at Nitride Heterointerfaces

5a. CONTRACT NUMBER

5b. GRANT NUMBER

5c. PROGRAM ELEMENT NUMBER
NISE

6. AUTHOR(S)

Andrew C. Lang

5d. PROJECT NUMBER

5e. TASK NUMBER

5f. WORK UNIT NUMBER
N20S

7. PERFORMING ORGANIZATION NAME(S) AND ADDRESS(ES)

Naval Research Laboratory
4555 Overlook Avenue, SW
Washington, DC 20375-5320

8. PERFORMING ORGANIZATION REPORT NUMBER

NRL/6360/MR--2023/3

9. SPONSORING / MONITORING AGENCY NAME(S) AND ADDRESS(ES)

Naval Research Laboratory
4555 Overlook Avenue, SW
Washington, DC 20375-532

10. SPONSOR / MONITOR'S ACRONYM(S)

NRL-NISE

11. SPONSOR / MONITOR'S REPORT NUMBER(S)

12. DISTRIBUTION / AVAILABILITY STATEMENT

DISTRIBUTION STATEMENT A: Approved for public release; distribution is unlimited.

13. SUPPLEMENTARY NOTES

Karles Fellowship

14. ABSTRACT

This report presents research conducted by Dr. Andrew C. Lang (Code 6366) during her Jerome and Isabella Karle Distinguished Scholar Fellowship from September 27th, 2021 – September 26th, 2022. It describes research into the interplay of strain and short range ordering at nitride heterointerfaces. The two material systems under examination here include high Sc-fraction ScAlN and cubic-boron nitride. Both of these epitaxial systems represent the state of the art in nitride synthesis, and as a result there is little known about the complex interplay of local structural defect, strain, phase/growth relationships resulting from epitaxial growth. This work aids in identifying the path towards future nitride heterostructure development and opens the door for future detailed studies on the relationship on local compositional and chemical ordering in device based on nitride heterostructures.

15. SUBJECT TERMS

16. SECURITY CLASSIFICATION OF:			**17. LIMITATION OF ABSTRACT**	**18. NUMBER OF PAGES**	**19a. NAME OF RESPONSIBLE PERSON**
					Andrew C. Lang
a. REPORT	**b. ABSTRACT**	**c. THIS PAGE**	U	12	**19b. TELEPHONE NUMBER** *(include area code)*
U	U	U			(202) 767-6238

This page intentionally left blank.

Contents

This page intentionally left blank.

EXECUTIVE SUMMARY

This report presents research conducted by Dr. Andrew C. Lang (Code 6366) during his Jerome and Isabella Karle Distinguished Scholar Fellowship from September 27th, 2021 – September 26th, 2022. It describes research into the interplay of strain and short range ordering at nitride heterointerfaces. The two material systems under examination here include high Sc-fraction ScAlN and cubic-boron nitride. Both of these epitaxial systems represent the state of the art in nitride synthesis, and as a result there is little known about the complex interplay of local structural defect, strain, phase/growth relationships resulting from epitaxial growth. This work aids in identifying the path towards future nitride heterostructure development and opens the door for future detailed studies on the relationship on local compositional and chemical ordering in device based on nitride heterostructures.

This page intentionally left blank.

Interplay of Strain and Short Range Ordering at Nitride Heterointerfaces

1. INTRODUCTION

This report documents the research I performed and participated in during the period of September 27th 2021 through September 26th 2022 under the Jerome and Isabella Karle Distinguished Scholar Fellowship Program. While the research here spans several related topics and focus areas, the primary focus is on nitride wide/ultrawide band gap semiconductors and the heterojunctions between these materials that create electron channels in electronic devices. When growing dissimilar materials using epitaxial growth methods it is common to have defects and other imperfections at the heterojunction due to a myriad of effects, specifically here I have looked into the interplay of strain and short range ordering at these nitride heterojunctions. This is of vital importance to the development of novel RF and power electronic components serving Naval and Department of Defense needs. The efforts of this work have resulted new programs on which I am listed as a co-investigator, including a new 6.1 base program extending the ScAlN work looking into the integration of dissimilar materials to create novel hybrid electronics, and an externally funded program continuing the development of cubic boron nitride (c-BN) as a candidate ultrawide-band gap material in next-generation high power and high frequency electronic devices.

2. EXPERIMENTS

2.1 Strain Mapping Cubic Inclusions in High Sc-Percentage ScAlN

The unique properties of $Sc_xAl_{x-1}N$ thin films have attracted significant attention based on the potential for improved performance in next-generation solid-state and acoustoelectric RF devices [1]. $Sc_xAl_{x-1}N$ is formed by adding cubic ScN, Fm-3m, to wurtzite AlN, $P6_3mc$, which both softens the bonding and increases the polarization compared to AlN. High Sc compositions, x = 0.43, exhibit a 5x increase in piezoresponse compared to pure AlN making $Sc_xAl_{x-1}N$ an extremely attractive candidate for future broadband filters for 5G frequencies and beyond [2]. Recently, sputtered polycrystalline $Sc_xAl_{x-1}N$ films with $x > 0.27$ have been shown to exhibit ferroelectricity, providing evidence that $Sc_xAl_{x-1}N$ may be the first experimentally demonstrated nitride ferroelectric [3]. Controlling the phase of epitaxially grown $Sc_xAl_{x-1}N$ is very challenging due to the interplay of misfit strain, Sc incorporation during growth, and the effect these factors have on the hexagonal/cubic phase boundary in the $Sc_xAl_{x-1}N$ alloy phase diagram.

Manuscript approved May 8, 2023.

Transmission electron microscopy analysis is ideally suited to examine the local structural morphologic, defect, and phase/growth relationships resulting from film epitaxial growth.

ScAlN alloys are predicted to be thermodynamically stable in the wurtzite phase for Sc-percentages as high as 55% ($Sc_{0.55}Al_{0.45}N$,) however this has not been experimentally realized with many phase pure wurtzite films being observed for Sc-percentages of 43% and lower [4]. Here we explore the structural morphology of the growth of $Sc_{0.40}Al_{0.60}N$ by molecular beam epitaxy and develop a workflow for rapid strain analysis across large areas of epitaxial films.

2.1.1 Results

Initially I examined an attempt at growing phase pure $Sc_{0.40}Al_{0.60}N$. *In situ* reflection high-energy electron diffraction indicated that the film growth started with a significant cubic character, and later transitions to the desired wurtzite phase. STEM imaging, as shown in figure 1, reveals the complex microstructural growth. Low magnification imaging, 1a, shows that the initial the film growth proceeds with narrow columnar domains that coarsen into larger domains with several inclined threading dislocations. It's interesting to note that, while the entire film contains threading dislocations, the threading dislocations at the top of the film are inclined, at approximately 72 degrees. Looking back through III-V literature, inclined threading dislocations in early research on AlGaN growth were found to indicate strain relief and the same factors are at play here [5]. Closer examination with high resolution high-angle annular dark-field imaging, 1b, confirms the RHEED observations. Cubic inclusions are found among the initial columnar growth features, and occasional few-nm cubic grains are also found throughout the coarser grained regions of film. Energy-dispersive x-ray spectroscopy (EDS) mapping confirms the expected x = 0.4 composition of the film, with no clear difference between cubic and hexagonal ScAlN grain compositions, which itself is a surprising result. While the globally averaged composition would reasonably be expected to be $Sc_{0.40}Al_{0.60}N$, it is surprising that the composition is the same no matter the morphology or phase of the film. Taking a closer look at the ScAlN/AlN interface, 1b, we can easily observe some small cubic grains throughout the region closest to the interface shown in blue boxes. These gains dot the interface throughout the sample, there is an average of about 10-15 nm between these cubic inclusions, and in some regions they can extend 10s of nm into the film. Analysis of the fast Fourier transform allowed me to index several unexpected reflections to rock salt ScN.

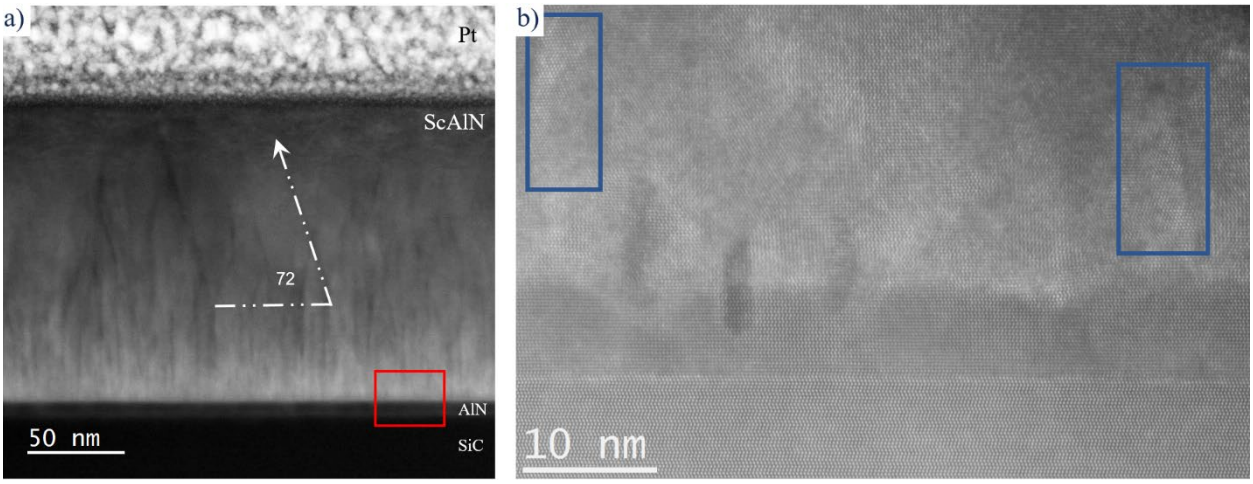

Figure 1. STEM imaging of epitaxially grown $Sc_{0.4}Al_{0.6}N$ film. a) low magnification HAADF image showing the complex microstructure present in the grown film. Note the columnar domains at the bottom of the film which transition to larger domains with inclined threading dislocations highlighted in the film. b) is from the area shown in red in a), and shows a high resolution HAADF image near the $AlN/Sc_{0.4}Al_{0.6}N$ interface. Cubic $Sc_{0.4}Al_{0.6}N$ inclusions are shown in the blue boxes.

While the EDS did not find any difference between the cubic and hexagonal ScAlN grains, there is a difference observable using electron energy loss spectroscopy (EELS) as shown in figure 2. The main ScAlN edge, shown in 2b, is intense and clearly observable although it is not easily interpretable. Due to the convolution of the Sc L- (at 406eV) and N K (at 402eV) edges direct interpretation of the edge feature observed at 402eV is challenging, but care examination shows that the cubic phase experiences a clear shift of 0.6eV to higher energy. This difference is small but clearly measurable and can serve as a fingerprint of each phase. The different morphology is likely due to the different bond distributions in the cubic and hexagonal lattices which is reflected in the EEL spectra.

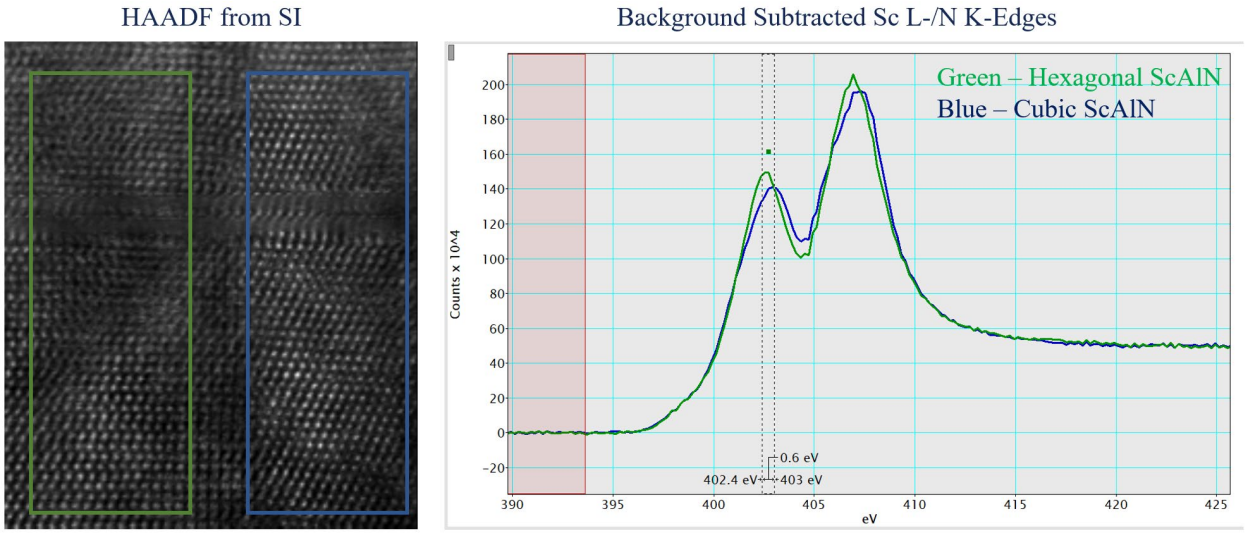

Figure 2. HAADF imaging and EELS analysis of the cubic and hexagonal $Sc_{0.4}Al_{0.6}N$ grains. Left, shows the simultaneously acquired HAADF image from the EELS SI clearly showing the two different phases. Right, extracted equal area EELS maps from the same SI shown on the left of the two different phases. The convoluted Sc L-/N K-edges shown here are background subtracted and overlaid, no other process was done to the data.

Strain analysis was performed using the newly acquired STEMx 4D-STEM attachment on the JEOL 2200FS. For this experiment the scope was aligned in STEM mode, using a 0.7 nm probe setting and the smallest CL aperture giving a convergence angle of approximately 4 mrad. The use of a small CL aperture limits the spatial resolution of the technique, due to the smaller convergence angle, but this has the effect of creating discrete disks in the convergent beam electron diffraction pattern. These disks are more easily able to be tracked and analyzed later in the processing steps. 4D STEM takes advantage of the fast refresh rate of the OneView camera on the TEM and allows us to acquire an electron diffraction pattern rapidly across thousands of probe positions.

The diffraction patterns are then compiled into a data cube very similar to that of EELS spectrum imaging. After acquisition the data cube can be analyzed by performing several preparation steps, detailed in figure 3, which I have chosen to do using Python; first aligning first beam drift and then fitting two apertures, *v* and *u* across the proper crystal axes in order to select the directions for the calculation of the 2-dimensional strain tensor. Further processing the data set results in spatially localized maps showing the 4 components of the 2-dimensional strain tensor. The red box in figure 3 shows the area selected as a reference, this area of the film was selected as a reference because it contained only a single wurtzite grain. What is immediately apparent is that there quite a lot of E_{XX} strain and many fewer areas of E_{YY} strain, this is expected due to the epitaxial growth of the film. This visually identifies areas with relaxed ScAlN grains in the film. E_{XY} is also of note, as the areas where it shows increased strain also tends to identify ScN rock salt inclusion type grains, suggesting that these grains form in regions of high strain. This clearly shows the power of strain analysis with 4D-STEM and the workflow developed for this material set is easily applied to numerous other single crystalline material systems.

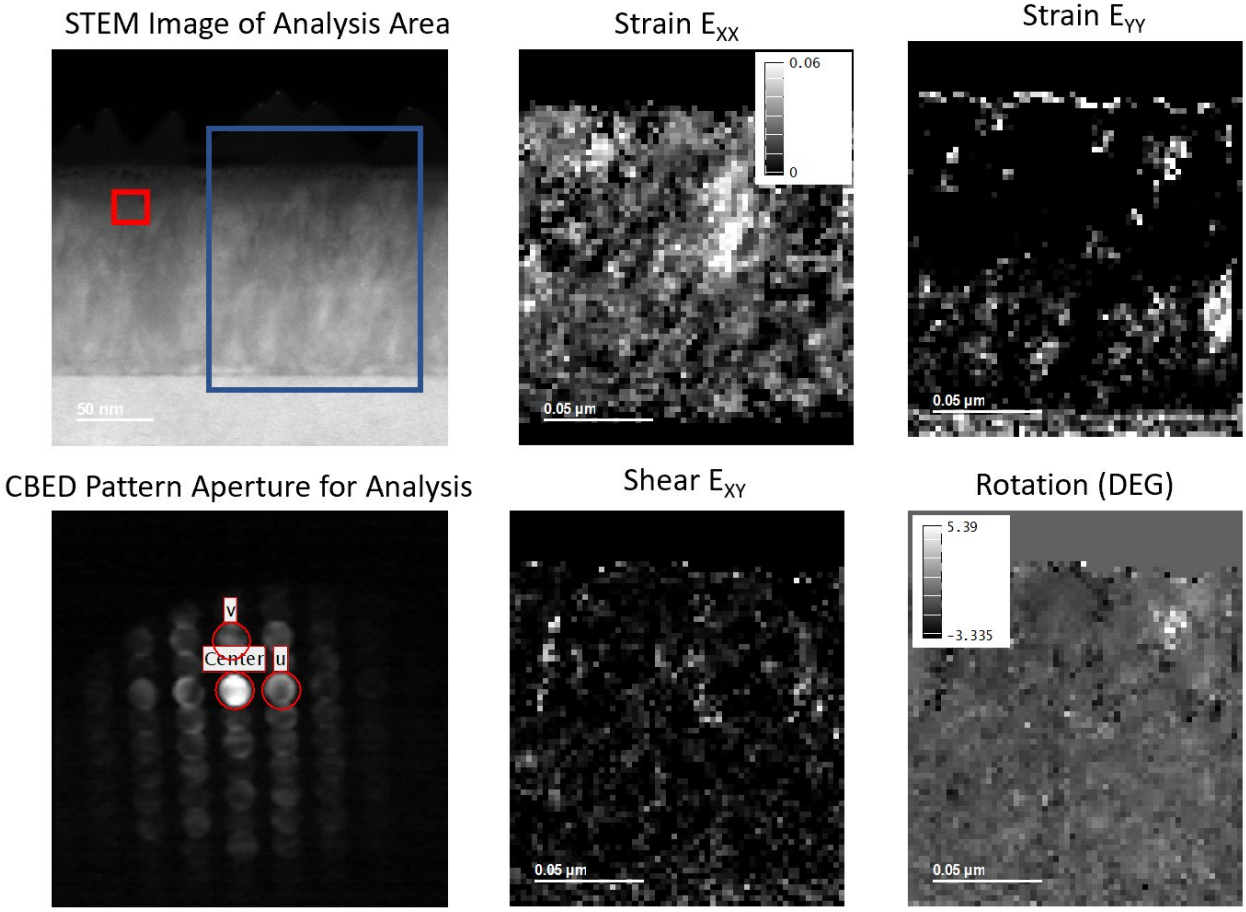

Figure 3. The workflow and typical output of a 4D-STEM Strain Analysis routine on ScAlN. Left, the TEM, aligned in STEM mode, selects an area and acquires a reference convergent beam electron diffraction pattern (CBED), then an area is identified and a CBED spectrum image is acquired. After acquisition the CBED spectrum image is centered, and two apertures are fit for strain analysis. Center and right, the output of the analyses after processing are spatially localized maps of the 2-dimensional strain tensor allowing for nm scale localized measurements of strain in single crystalline specimens.

2.1.2 Conclusions and Future Directions

These results are being complied into a manuscript. Initial attempts at growing a graded $Sc_{0.32}Al_{0.68}N/Sc_{0.4}Al_{0.6}N$ film have resulted in lower strain and suppressed cubic inclusion formation. This work is still ongoing and has relevance to a newly funded base program, on which I am CO-I that will continue working on ScAlN and integration of dissimilar materials to create novel hybrid electronics. The 4D-STEM workflow routine developed in house will continue to be optimized with features added in the future. In particular, future work includes developing the ability to discriminate different material phases from 4D-STEM spectrum images automatically from aligned data sets.

2.2 Phase purity and defects present in MBE grown c-BN

Demand for devices with greater efficiency comes in many forms. Wide-band gap materials (E_g > 3.3 eV) like gallium nitride have succeeded in offering advantages over conventional devices by offering higher breakdown voltages, operating frequencies, and thermal conductivity. Ultrawide-band gap materials promise even greater performance benefits. Among the group-III nitrides, cubic boron nitride (c-BN) is a promising candidate material due to its large band gap (E_g > 6.1eV), high thermal conductivity, and ability to be doped either *p*- or *n*-type. In spite of many efforts c-BN is still the least mature of the ultrawide-band gap materials [6]. This is primarily due to the difficulties in synthesizing high-quality phase pure c-BN crystals and the large number of unintentional defects present in grown crystals. Aberration-corrected scanning transmission electron microscopy (STEM) is ideally suited to examine the local structural morphologic, defect, phase/growth relationships, and dopant integration in c-BN epitaxial growth.

Here I examine the structure and film morphology the recently successful growth of c-BN on diamond at NRL. Using a combination of aberration corrected STEM imaging and EELS I can identify the typical defects in the structure and by using advanced EELS analysis better understand how the changes in EEL fine-structure reflect changes in the local short range ordering the c-BN.

2.2.1 Results

In this work, I examined c-BN films grown on diamond via molecular beam epitaxy with post-growth cross-sectional STEM. After confirming the presence of c-BN with fourier transform infrared spectroscopy samples were analyzed in a Nion UltraSTEM 200X, with a convergence angle of 27 mrad. EELS was performed at 60 kV while imaging was done at both 60 and 200 kV. The use of different accelerating voltages is due to the fact that, similar to graphene, the knock-on damage threshold for c-BN is approximately 100kV, and beyond 100kV the material degrades under the beam. While the damage is not immediate, during the long exposures, 0.02ms for EELS compared to 0.005ms for imaging, there was enough incident electron beam current to damage both the EELS fine-structure and drill holes into the c-BN.

An unexpected challenge of analyzing c-BN on diamond in the TEM was related to sample preparation. Diamond is well known as one of the hardest materials, and while c-BN is also very hard the two materials mill very differently during sample preparation in the focused ion beam (FIB). The hardness of the diamond, first and foremost, limits sample preparation choices to just the use of

FIB, traditional grinding and polishing is impossible. Unfortunately, initial attempts at making samples in the FIB resulted in samples with 2 major issues: 1. An extremely large amount of Ga-damage across the sample smothering out the contrast from the much lighter elements C, B, and N within the film, and 2. the extreme difficulty in making flat, as opposed to sharply wedge shaped, samples with uniform thickness for reliable EELS analysis. These issues were overcome in two ways: 1. Use of a precision Argon Ion Milling system in order to clean up and remove Ga-beam damage from the FIB and 2. The development of a unique routine of sample preparation for c-BN samples in the FIB. The sample preparation routine includes the steps of the traditional *in-situ* liftout routine in the FIB up to the point where the lamella has been lifted out and is on the nanomanipulator needle. At this point the sample is rotated 90 degrees on the nanomanipulator needle and is welded to a sacrificial post. Then, the sample stage is rotated 180 degrees and the lamella is picked back up, and rotated another 90 degrees and is then welded to the post for further sample preparation. This has the effect of turning the sample upside down, thereby allowing for the extremely hard diamond to be used as a sacrificial layer during sample preparation. This greatly suppresses the wedge formation of the sample during preparation and produces a much more uniform sample for highly sensitive EELS measurements. The only drawback of this technique is that it leaves a very small amount of diamond left after thinning to electron transparency, this makes tilting to an appropriate zone axis quite challenging.

Annular bright-field imaging, shown in figure 4, reveals the presence of a high density of stacking faults, which appear in the image as diagonal features inclined 55° to the growth plane. Unlike ScAlN these defects are not indicative of strain relief, but are common stacking faults in FCC crystals. The c-BN/diamond interface is abrupt, with occasional misfit dislocations, further analysis of the EELS near edge structure of the B K-edge identifies a small pre-peak feature ~191.3 eV. This edge feature has previously been attributed to a bound exciton originating from the π* orbital, and in h-BN is a strong feature equal in intensity to the main edge feature at ~197 eV [7, 8]. π* states are absent in the cubic phase due to bond hybridization; therefore, the weak presence of this feature indicates the that the nucleating BN layer contains h-BN like bonding while still maintaining the cubic phase.

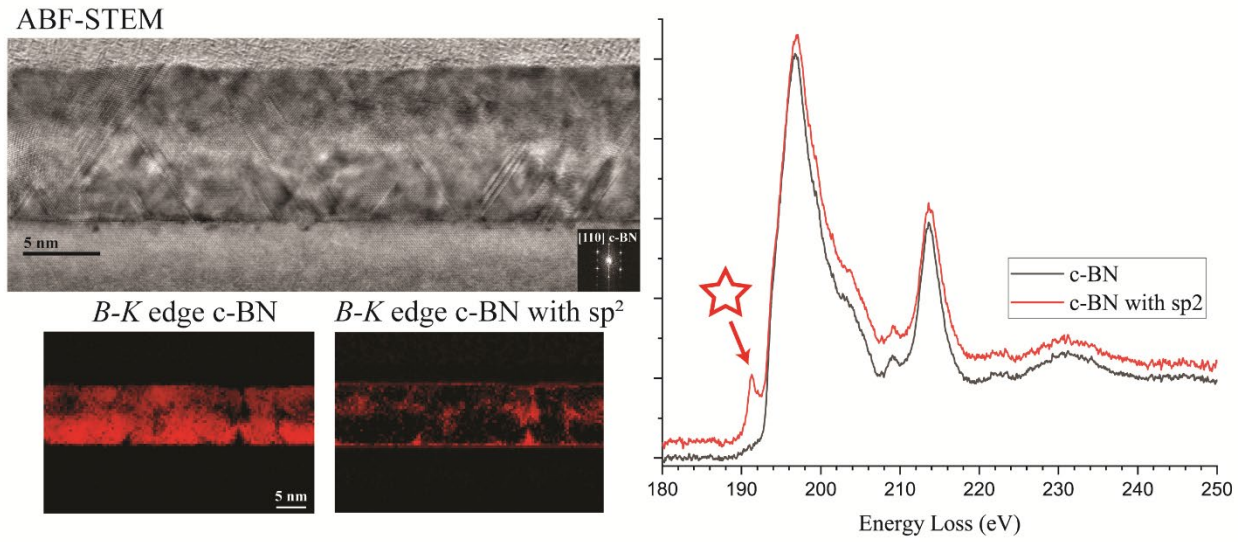

Figure 4. Cross-sectional STEM analysis of c-BN. Top: Annular bright-field STEM image of the c-BN thin film. Bottom: EELS maps showing where individual spectra features of the B K-edge are observed; left, typical c-BN spectra; right, c-BN spectra with a pre-peak feature at 191eV, indicative of the presence of small amounts of sp^2 bonding in the BN. The EEL spectra shown on the right were processed with a power law background subtraction and slightly offset for visual clarity.

The installation of the MerlinEELS direct electron detector was delayed, only being installed in late June 2022. This impacted progress on developing an extended electron energy-loss fine structure (EXELFS) workflow, progress is ongoing. Early data is highly promising and the increased sensitivity has already revealed new features buried in the EEL fine-structure of c-BN. New data collected using the MerlinEELS detector is shown in figure 5. We earlier identified a pre-peak feature at 191.3 eV of the B *K* edge and attributed it to a small amount of π^* states indicating some h-BN like bonding in the structurally cubic c-BN material. While this edge feature was present in the B *K* edge, the greater energy field of view offered by the MerlinEELS detector informed us that there were no fine-structural changes visible on the N *K* edge, leading to some concerns about the nature of this 191.3 eV feature, as the N *K* edge of h-BN and c-BN are easily distinguishable [8]. If there was bond hybridization present both the B and N *K* edges would have a prepeak visible, which can be observed in the black spectra in 5 where both B and N have prepeak features. In many areas, denoted by white in the colored EELS map in figure 5, there was the presence of the peak in the B *K* edge but not in the N *K* edge. This led to further analysis which revealed that the edge fine-structure in this area is like identifying a large agglomeration of point defect, specifically V_N [9].

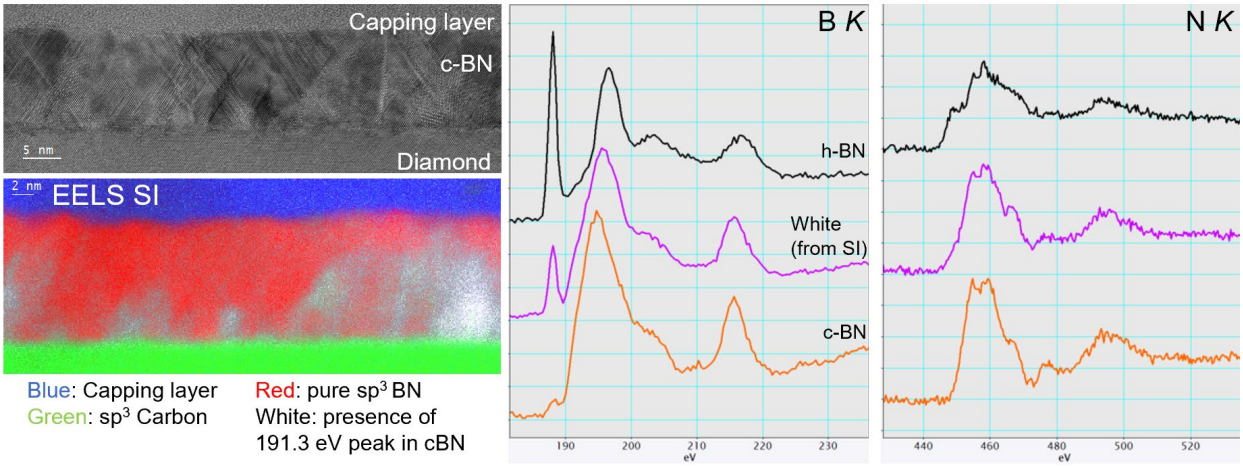

Figure 5. Cross-sectional STEM analysis of c-BN. Top left: Annular bright-field STEM image of the c-BN thin film. Bottom left: Colorized EELS map showing where individual spectral features of the B K-edge are observed; right, representative BN spectra including both B and N *K* edges, note the presence or absence of changes in the bonding of both the cation and anion spectra; The colorized EELS map was processed by first identifying the edge features in the raw data then separately mapping their relative intensity with MLLS fitting before creating a color map. The EEL spectra shown on the left were processed with a power law background subtraction and offset for visual clarity.

2.2.2 Conclusions and Future Directions

These results were in part published [10] and presented at the 2022 Microscopy and Microanalysis conference [11] the rest of the results are being compiled into a manuscript. This work is continuing with

external funding to continue the development of c-BN as a candidate material in next-generation high power and high frequency electronic devices. Development of the EXELFS workflow is continuing. Further exploration of the EELS fine-structure of c-BN is ongoing with a focus on the structure of defects within c-BN and their impact on heterostructure electrical performance.

3. SUMMARY

The work done on these two material systems helps lay the ground work for further development of in-house techniques to measure strain on the nanometer scale and analyze short range order in novel nitride heterostructures. In the future, further experimental characterization will be combined with the tools and techniques developed here better understand electronic device behavior and clearly identify any nanoscale phenomena that may be challenging to interpret from lower spatial resolution techniques.

Lastly, I would like to thank my former postdoc supervisor Rhonda Stroud, who advocated for me to become a Karles Fellow and provided crucial guidance over the past 3+ years at NRL. I would also like to acknowledge several of my NRL collaborators who helped design, grow, and characterize the samples described here, in no particular order, Eric Jin, Matthew Hardy, Neeraj Nepal, David Storm, Ginger Wheeler, and David Meyer.

REFERENCES

[1] M. Hardy, E. Jin, N. Nepal, D. S. Katzter *et al* 2020 Appl. Phys. Express 13 065509

[2] M. Akiyama, K. Kano, A. Teshigahara, Appl. Phys. Lett., 95 (2009) 162107.

[3] S. Fichtner, N. Wolff, N. Lofink, *et al* Appl. Phys., 125 (2019) 114103.

[4] S. Zhang, D. Holec, W.Y. Fu, C.J. Humphreys, M.A. Moram, J. Appl. Phys., 114 (2013) 133510.

[5] Follstaedt, D. M. et al. Appl. Phys. Lett. 87, 121112 (2005)

[6] N. Izyumskaya, D. O. Demchenko, S. Das, Ü. Özgür, V. Avrutin, and H. Morkoç, Adv. Electron. Mater. 3, 1600485 (2017)

[7] P. Widmayer, H.G. Boyen, P. Ziemann, P. Reinke, and P. Oelhafen, Phys Rev B 59, 5233 (1999)

[8] X.W. Zhang, H.-G. Boyen, N. Deyneka, P. Ziemann, F. Banhart, and M. Schreck, Nature Mater. 2, 312 (2003)

[9] McDougall et al. MRSF16-2560623.R1

[10] Storm, D.F., Maximenko, S.I., Lang, A.C., Nepal, N., Feygelson, T.I., Pate, B.B., Affouda, C.A. and Meyer, D.J. (2022), Mg-Facilitated Growth of Cubic Boron Nitride by Ion Beam-Assisted Molecular Beam Epitaxy. Phys. Status Solidi RRL, 16: 2200036

[11] Lang, A., Storm, D., Maximenko, S., Nepal, N., Meyer, D., & Stroud, R. (2022). Probing Defects in Epitaxially Grown Cubic Boron Nitride on Diamond. Microscopy and Microanalysis, 28(S1), 2382-2383